

A comparison of empirical and neural network approaches for estimating corn and soybean leaf area index from Landsat ETM+ imagery[☆]

Charles Walthall^{a,*}, Wayne Dulaney^a, Martha Anderson^b, John Norman^b,
Hongliang Fang^c, Shunlin Liang^c

^aUSDA-ARS Hydrology and Remote Sensing Laboratory, Building 007, BARC-West, Room 120B,
10300 Baltimore Boulevard, 20705-2350, Beltsville, MD, USA

^bDepartment of Soil Science, University of Wisconsin, Madison, WI, USA

^cDepartment of Geography, University of Maryland, College Park, MD, USA

Received 9 October 2003; received in revised form 4 June 2004; accepted 5 June 2004

Abstract

Plant foliage density expressed as leaf area index (LAI) is used in many ecological, meteorological, and agronomic models, and as a means of quantifying crop spatial variability for precision farming. LAI retrieval using spectral vegetation indices (SVI) from optical remotely sensed data usually requires site-specific calibration values from the surface or the use of within-scene image information without surface calibrations to invert radiative transfer models. An evaluation of LAI retrieval methods was conducted using (1) empirical methods employing the normalized difference vegetation index (NDVI) and a new SVI that uses green wavelength reflectance, (2) a scaled NDVI approach that uses no calibration measurements, and (3) a hybrid approach that uses a neural network (NN) and a radiative transfer model without site-specific calibration measurements. While research has shown that under a variety of conditions NDVI is not optimal for LAI retrieval, its continued use for remote sensing applications and in analysis seeking to develop improved parameter retrieval algorithms based on NDVI suggests its value as a “benchmark” or standard against which other methods can be compared. Landsat-7 ETM+ data for July 1 and July 8 from the Soil Moisture EXperiment 2002 (SMEX02) field campaign in the Walnut Creek watershed south of Ames, IA, were used for the analysis. Sun photometer data collected from a site within the watershed were used to atmospherically correct the imagery to surface reflectance. LAI validation measurements of corn and soybeans were collected close to the dates of the Landsat-7 overpasses. Comparable results were obtained with the empirical SVI methods and the scaled SVI method within each date. The hybrid method, although promising, did not account for as much of the variability as the SVI methods. Higher atmospheric optical depths for July 8 leading to surface reflectance errors are believed to have resulted in overall poorer performance for this date. Use of SVIs employing green wavelengths, improved method for the definition of image minimum and maximum clusters used by the scaled NDVI method, and further development of a soil reflectance index used by the hybrid NN approach are warranted. More importantly, the results demonstrate that reasonable LAI estimates are possible using optical remote sensing methods without in situ, site-specific calibration measurements.

© 2004 Elsevier Inc. All rights reserved.

Keywords: LAI; Landsat ETM+; NDVI; SVI; Green SVI; Neural network; LUT; SMEX; AERONET; Vegetation cover

1. Introduction

Foliage density expressed as leaf area index (LAI) is a critical parameter for many agronomic, ecological, and meteorological applications. Estimates of LAI are used in

plant growth models, energy balance models, climate models, and as a means of quantifying crop variability for precision farming. Reasonable estimates of LAI over large areas are needed for applications such as global climate change predictions.

Accurate estimates of LAI can also be used to compensate for the effects of vegetation moisture and vegetation architecture on microwave remote sensing estimates of soil moisture (Engman & Chauhan, 1995). Thus, near-simultaneous estimates of regional LAI are needed to derive satellite-based estimates of soil moisture from radar data.

[☆] Mention of company names is for information purposes only and does not constitute endorsement to the exclusion of others.

* Corresponding author. Tel.: +1-301-504-6074; fax: +1-301-504-8931.

E-mail address: cwalthall@hydrolab.arsusda.gov (C. Walthall).

Accurate LAI maps of the Soil Moisture EXperiment 2002 (SMEX02) study area were needed for input to soil moisture retrieval algorithms as part of the experiment (Jackson, 2002). An important consideration for the selection of SMEX02 LAI retrieval methods was to address algorithms potentially suitable for operational estimates of soil moisture from satellites. Reasonable accuracy and repeatability of LAI estimates, computational simplicity, and most importantly, minimal calibration requirements for use in diverse geographic locations are among the desirable attributes of operational algorithms.

Optical remote sensing is an economically feasible way to retrieve information such as LAI on regional to global scales at acceptably high spatial and temporal frequencies (Verstraete et al., 1996). A variety of approaches have been developed for calculating LAI over large areas from remotely sensed optical imagery: (1) empirical (parametric statistics) correlations between surface-measured LAI and spectral vegetation indices (SVI), (2) inversion of LAI from physically based canopy reflectance models, and (3) estimation using a neural network (NN) approach. The results from these procedures vary by scale of observation, type of vegetation, spectral bands used, and the sophistication of the models. Image calibration and atmospheric correction can also affect results. A recurring issue that inhibits the use of traditional LAI retrieval approaches is that they often need to be optimized for a specific geographic location or vegetation type to be used successfully.

There are disadvantages associated with each approach. Retrieval of LAI using empirical approaches, which establish a correlation between SVI and the biophysical parameter of interest, tends to be site-specific. Empirical relationships are valid only under conditions similar to those at the time the correlation was established. The relationship may break-down if the solar and viewing geometries, soil background, chlorophyll concentrations, or moisture conditions are different (Jacquemoud et al., 1995). Additionally, in situ calibration measurements of LAI over regional or global scales are impractical.

Retrieval of LAI through inversion of physically based canopy reflectance models is computationally very cumbersome for large geographic areas. There is no universally applicable canopy reflectance model for all vegetation types, thus making model selection problematic. Model selection is often a compromise between model complexity, invertibility, and computational efficiency (Jacquemoud et al., 1995). One-dimensional radiative transfer models are best suited to inversion, but they often have the tendency to oversimplify. Associated problems can include lack of convergence, sensitivity of results to initial values chosen for the solution, and difficulty in estimating model input parameters that cannot be directly measured. For example, Eklundh et al. (2001) found that inversion of LAI from Landsat-7 ETM+ data was especially difficult because of the large number of model input parameters needed as well

as the uncertainty associated with estimating some of the parameters.

Neural network approaches have not been generalized to handle arbitrary directional and spectral combinations (Smith, 1993; Fang et al., 2003; Kimes et al., 1998). Observations that are used to train the NN must encompass the expected range of values for the landscape under investigation. The availability of a large, surface-measured, vegetation data set of high quality is therefore necessary for the validation of the NN approach over large areas. An advantage of the NN approach is that it allows the use of complex, detailed models that would not be suitable for classical inversion due to very slow inversion times (Jacquemoud et al., 2000). Furthermore, NN approaches are not as affected by initial choices as traditional model inversion approaches are, nor are they as computationally intensive as traditional techniques. Forward runs of the NN are fast once NN training is completed.

Promising variations of the above approaches include within-scene scaling of an SVI that yields LAI directly as a function of the fraction of vegetation cover (Campbell & Norman, 1998; Choudhury et al., 1994) and a hybrid radiative transfer-neural network (RT-NN) approach (Fang & Liang, 2003). The hybrid method has been used to retrieve LAI of grasses, crops, and forests using Landsat-7 ETM+ top-of-atmosphere radiances as well as atmospherically corrected surface reflectances. Both the scaled normalized difference vegetation index (NDVI) and the hybrid method require little or no in situ calibration measurements and are thus potential solutions for global operational systems.

The objective of this study was to evaluate a variety of approaches for the retrieval of LAI from Landsat-7 ETM+ data of the SMEX02 study area. These techniques include the RT-NN hybrid and scaled SVI methods, an empirical approach using NDVI, and an empirical approach using a SVI incorporating green wavelengths as reported by Gitelson et al. (in press).

The normalized difference vegetation index (NDVI) has been an extremely popular SVI for biophysical parameter retrieval (Rouse et al., 1973). NDVI has been used at virtually all scales ranging from small plot research to global investigations. Part of its popularity stems from the fact that it uses baseline spectral bands available from virtually all remote sensing systems, including color infrared photography, and it is computationally very efficient. Although numerous investigations have shown that NDVI is not the best solution for LAI retrieval under all circumstances, its use persists in the literature and is popular among operational users of remote sensing data (Best & Harlan, 1985; Carlson & Ripley, 1997; Colombo et al., 2003; Myneni et al., 1995; Spanner et al., 1990). The continued widespread acceptance of NDVI by both the application and research communities suggests that NDVI is a suitable benchmark for comparing alternative biophysical parameter retrieval algorithms and solutions.

2. Algorithm descriptions

2.1. Empirical SVI methods

Empirical approaches for estimating LAI have traditionally used combinations of red and near infrared (NIR) wavelengths in SVIs such as NDVI. The NDVI is given as

$$\text{NDVI} = \frac{(\rho_{\text{NIR}} - \rho_{\text{Red}})}{(\rho_{\text{NIR}} + \rho_{\text{Red}})} \quad (1)$$

where ρ_{NIR} and ρ_{Red} are the NIR and red wavelength reflectances. A least squares regression using linear or curvilinear relationships between a sample of NDVI image pixels and surface-measured LAI is determined and then applied to the entire image. One limitation of NDVI is that it becomes asymptotic at LAI values between 2.0 and 3.0 and is therefore not responsive to further increases of LAI. The SVI reported by Gitelson et al. (in press) uses green wavelength reflectance instead of red reflectance and appears to remain sensitive to changing levels of vegetation at LAIs beyond 3.0. The Gitelson green index (GI) is given as

$$\text{GI} = \frac{(\rho_{\text{NIR}})}{(\rho_{\text{Green}})} - 1.0 \quad (2)$$

where ρ_{Green} is the green wavelength band reflectance.

2.2. Scaled SVI method

The scaled SVI approach links an SVI for a fraction of vegetation cover (f_c) reported by Choudhury et al. (1994) and Gillies and Carlson (1995) with an equation for LAI expressed as a function of f_c reported by Campbell & Norman (1998). Fraction of vegetation cover is calculated using

$$f_c = 1 - \left[\frac{\text{NDVI}_{\text{MAX}} - \text{NDVI}_i}{\text{NDVI}_{\text{MAX}} - \text{NDVI}_{\text{MIN}}} \right]^{0.6} \quad (3)$$

where NDVI_{MAX} is the maximum NDVI value for the image, NDVI_{MIN} is the minimum NDVI for the image, and NDVI_i is the NDVI of an individual pixel. The f_c is then used to calculate LAI via

$$\text{LAI} = -2\ln(1 - f_c) \quad (4)$$

As it is important to avoid including water pixels or spurious high value pixels when determining the minimum and maximum NDVI values, it is usually preferable to use the mean of the end 3% of the tails of the NDVI histogram for the minimum and maximum values. The scaled SVI approach assumes random orientation and distribution of leaves throughout the canopy with no clumping of elements. Note that the relationship between f_c and LAI is the basis for algorithms used by nondestructive LAI field measurement instrumentation widely accepted by the research community (Welles, 1990; Welles & Norman, 1991).

2.3. Hybrid method

Implementation of the RT-NN hybrid approach requires the creation of a simulation database or lookup table (LUT) that relates canopy biophysical parameters and viewing geometries to Landsat-7 ETM+ spectral reflectance. This database is subsequently used to train the neural network. The trained NN is then applied to atmospherically corrected imagery of surface reflectances to generate LAI. It is important that the canopy reflectance model inputs encompass the full range and combination of expected field conditions. To a large extent, the success of the NN predictions is based on how accurately the soil–plant–atmosphere continuum is physically modeled.

The Markov chain reflectance model (MCRM) (Kuusk, 1994) was used to create the simulation LUT. The MCRM is a turbid medium, analytical multispectral canopy reflectance model that calculates nadir reflectance in the 400- to 2500-nm range for homogeneous vegetation canopies. It was chosen because it is a physically based model that can be successfully run in the forward direction using input parameters from field measurements or from parameter values reported in the literature. An additional advantage of MCRM is that it can model plant canopies largely made up of vertical elements such as corn because it incorporates Markov properties of stand geometry. The MCRM incorporates the PROSPECT leaf radiative transfer model to simulate leaf optical properties (Jacquemoud & Baret, 1990). Soil reflectance is characterized by four basis functions as defined by Price (1990). The MCRM also incorporates a diffuse to total irradiation skylight ratio model.

Input values of LAI, a Markov clumping factor, and leaf spatial distribution are needed to characterize canopy structure. Other parameter inputs include leaf biochemical and structural properties (e.g., chlorophyll $a+b$ and the number of internal leaf layers), soil spectral reflectance and directional properties, the solar viewing geometry, and atmospheric turbidity.

A soil reflectance index (SRI) was used to retrieve soil reflectance from the imagery. The SRI is based on the linear relationship between red and near infrared reflectance of bare soil as described by the soil line (Baret et al., 1993). The soil line is actually a “buffer range” or “strip” at the base of the tasseled-cap structure of a red-near infrared scattergram of pixel values (Fang & Liang, 2003) (e.g. Fig. 3). The minimum and maximum reflectances of the soil line are calculated as the means of clusters with centers located typically at the 2% percentile (for the minimum) and the 98% percentile (for the maximum)

$$\rho_1 = \text{Mean}(S_1)$$

$$\rho_2 = \text{Mean}(S_2)$$

where ρ_1 and ρ_2 are minimum and maximum band reflectances derived from the soil line and S_1 and S_2 are the lower

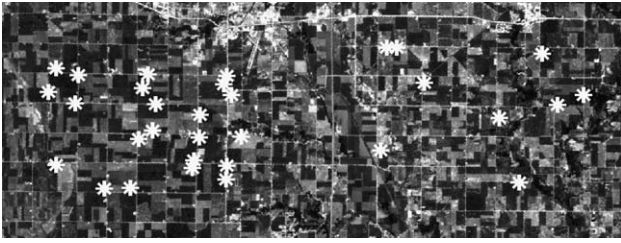


Fig. 1. Subset from the July 1, 2002 Landsat-7 ETM+ band 3 (red) image showing the Walnut Creek watershed. White stars indicate sites where ground-based LAI-2000 measurements were made.

and upper clusters of soil pixels for calculating ρ_1 and ρ_2 . SRI is given as

$$\text{SRI} = \frac{\rho_s - \rho_1}{\rho_2 - \rho_1} \quad (5)$$

The soil reflectance (ρ_s) for a pixel can be calculated using

$$\rho_s = \rho_{i1} + (\rho_{i2} - \rho_{i1})\text{SRI} \quad (6)$$

where ρ_{i1} and ρ_{i2} are the minimum and maximum values of soil reflectance of band I estimated by calculating the mean of the minimum and maximum soil pixel clusters as determined by visual inspection.

3. Data collection and processing

3.1. Study site description

The SMEX02 experiment was conducted in and around the Walnut Creek Watershed south of Ames, IA, during June and July, 2002 (Fig. 1). Approximately 95% of the land area

is used for agriculture. Corn and soybean are grown on approximately 80% of the row crop acreage, with greater than 50% in corn, 40–45% in soybean, and the remaining 5–10% in forage and grains. The watershed is representative of the Des Moines Lobe, which covers approximately 1 quarter of the state of Iowa. The climate is humid with an average annual rainfall of 835 mm. The experimental watershed has some of the youngest soils in the United States and is considered to be a part of the pothole region of Iowa because of the undulating terrain. There are two notable features of the landscape: (1) lack of a surface stream channel except for areas near streams and rivers and (2) significant variation of soil types within the spatial scale represented by a typical production field. Surface organic matter content can often range from 1–2% to over 8% within a single field as one follows a transect from pothole areas to eroded knolls. This variability is also associated with high variation of rooting depth. If the spring or summer is extremely wet, the soil surface can be randomly covered with water-filled potholes. These potholes are usually dry by early spring due to subsurface drainage and farmers are able to plant without difficulty. The inherent variability experimental watershed demanded that care be taken during the design of the sampling scheme to ensure that surface conditions within fields are adequately sampled.

3.2. Field data collection

Farm owners within the SMEX02 study area were contacted for permission to collect vegetation data from their fields. Color infrared aerial photography was used to help identify three areas within each field that were representative of low, average, and high vegetation amounts. The

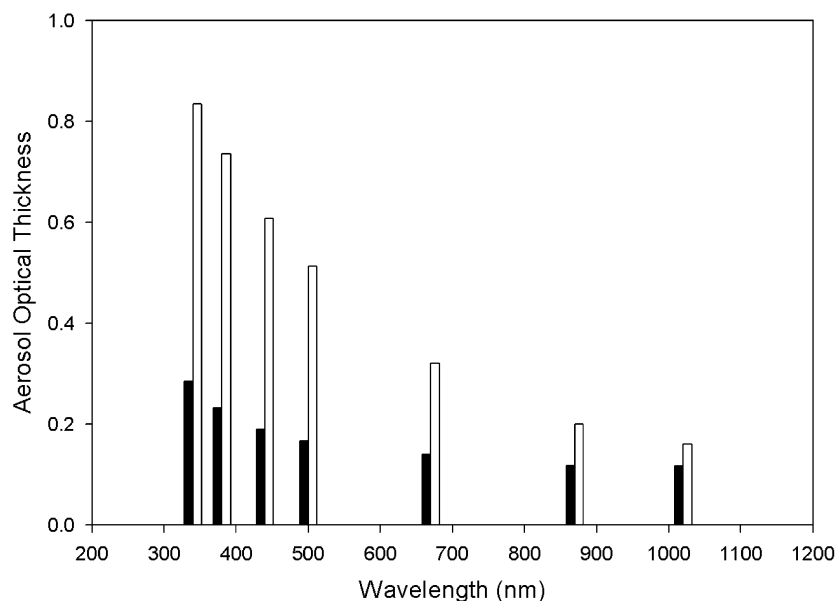


Fig. 2. Split-bar graph of the aerosol optical thickness for July 1 (black bar) and July 8 (white bar). Total precipitable water amounts were notably different for the two overpass dates: 3.3 cm for July 1 and 4.5 cm for July 8.

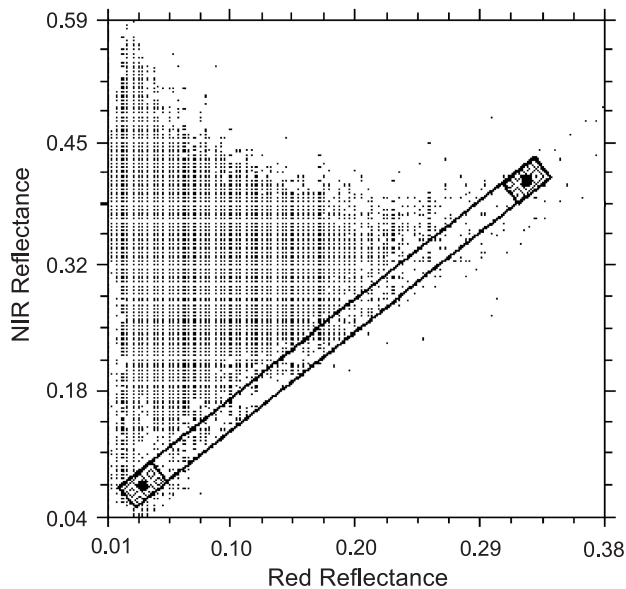


Fig. 3. Two-dimensional scatter plot of July 1 Landsat-7 ETM+ red and NIR surface reflectances. The minimum and maximum soil reflectance values were obtained by calculating the mean (black dot) of the lower 2% and upper 98% cluster of cells (hatched shading) at the ends of the “soil strip”.

mean of five LAI measurements collected at each site was considered the best estimate of LAI for that particular day and location. A total of 94 sample sites across the entire experimental watershed were measured for LAI (Anderson et al., 2004).

Corn and soybean LAIs were collected using the nondestructive optical methods of Welles and Norman (1991) and Li-Cor. (1992). Using this approach, the resulting LAI measurement yields a foliage area index that includes standing green foliage LAI, standing non-green foliage LAI, and non-foliage canopy architectural components such as stalks, fruit, and branches. Assumptions of the algorithm include (1) random positioning of small foliage elements within the canopy and also with respect to azimuth and (2) only sky radiation is seen by the sensors when positioned beneath the canopy. The procedure permits rapid LAI measurements from multiple canopies and locations.

3.3. Landsat-7 ETM+ imagery

Landsat-7 ETM+ imagery was acquired throughout the duration of the SMEX02 field experiment. The ground instantaneous field of view of the ETM+ imagery is 30 m. Cloud-free ETM+ overpasses from July 1 to July 8 were chosen for analysis. Two Landsat-7 images 1 week apart were available because the study area falls within the overlap area of adjacent satellite tracks (i.e., paths 26 and 27; row 31).

The 520–600 nm (green, band 2), 630–690 nm (red, band 3), and 760–900 nm (near infrared, band 4) channels of both Landsat-7 ETM+ scenes were converted from spectral radiance to surface reflectance prior to analysis. The second simulation of the satellite signal in the solar spectrum (6S) atmospheric radiative transfer model was chosen to perform atmospheric correction of the ETM+ scenes and for calculation of surface reflectance (Vermote et al., 1997). Input parameters for 6S include solar and sensor view angle geometries, target and sensor elevations, ozone concentration, spectral aerosol optical depth, total precipitable water, aerosol volume, and aerosol size distribution.

A sunphotometer borrowed from the AEROSOL ROBOTIC NETWORK (AERONET; Holben et al., 1998) was centrally located within the study area. The AERONET sunphotometers are automatic solar-tracking spectral radiometers that collect narrow field of view (1.2°) direct sun and sky radiance measurements of aerosol optical properties at 340, 380, 440, 500, 675, 870, 940, and 1020 nm. After data quality checks and cloud screening were performed, these measurements were used to calculate atmospheric aerosol size distribution, aerosol refractive indices, aerosol optical depth at 550 nm (logarithmic interpolation between measured aerosol optical depths at 500 and 675 nm), and precipitable water (Eck et al., 1999). Atmospheric ozone measurements were obtained from the World Ozone and Ultraviolet Data Center (<http://www.msc-smc.ec.gc.ca/woudc/index.html>). Aerosol optical depths from July 1 to July 8 are presented as Fig. 2. Note the higher aerosol optical depth values and precipitable water contents for July 8. SMEX02 field participants reported visual observations of “smoke in the air” on that date. It was later

Table 1
Performance of the LAI retrieval methods

Index	Date	Percent R/V	r^2	RMSE	n	O	P	MBE	Percent error
Scaled	07-01-02	N/A	0.72	0.41	72	2.50	2.36	−0.14	22.5
Scaled	07-08-02	N/A	0.48	0.45	60	3.13	2.88	−0.25	27.0
Gitelson	07-01-02	65/35	0.79	0.53	27	2.62	2.41	−0.21	21.2
Gitelson	07-08-02	65/35	0.38	1.27	21	3.04	3.16	0.12	30.7
NDVI	07-01-02	65/35	0.87	0.44	25	2.57	2.41	−0.16	18.57
NDVI	07-08-02	65/35	0.48	1.26	21	3.04	2.21	−0.83	66.7
NN	07-01-02	N/A	0.63	0.63	83	2.50	2.94	0.44	17.5
NN	07-08-02	N/A	0.40	0.70	67	3.10	3.13	0.03	0.9

Here Percent R/V is the percentage of the SVI/LAI dataset used for regression and validation, r^2 is the coefficient of determination, RMSE is the root mean square error, n is the number of observations, O is the mean observed value, P is the mean predicted value, and MBE is the mean-bias-error.

confirmed that large forest fires in Colorado during the summer of 2002 were the source of the smoke.

Bands 3 and 4 of the atmospherically corrected Landsat-7 ETM+ image were used to compute NDVI. Bands 2 and 4 were used to compute GI. A 65% subset of the data was used to calculate regression equations, with the remaining data used to validate the results.

The LUTs for corn and soybeans were created by forward runs of the MCRM. Input parameters (excluding the solar zenith angle at the time of the satellite overpass and soil reflectance values determined directly from the ETM+ imagery for calculation of the SRI) were obtained from values reported by Fang and Liang (2003). Their values were obtained through inversion of ETM+ imagery acquired over the eastern half of the state of Maryland and fell within the range of values reported by other investigators (Kuusk, 1995). MCRM was run using multiple values for the solar zenith angle (10–70° by a 10° step) and LAI (0.0–10.0 by a 0.1 step). The minimum and maximum soil reflectance values used for the calculation of SRI were determined from the soil line as revealed in the 2D spectral plot of red and near infrared surface reflectances from the SMEX02 ETM+ imagery (Fig. 3). A feed-forward, back-propagating NN was trained on the LUT (Venables & Ripley, 1994).

Validation LAI values for comparison with LAI estimates from the July 1, 2002 Landsat-7 ETM+ image were obtained by interpolating between ground base LAI measurements made immediately before and after the satellite overpass date. Linear interpolation could not be used to derive the LAI ground data for comparison with the July 8 image because vegetation sampling did not occur after the 8th. As a result, those LAI measurements acquired immediately before the July 8 overpass were used to make up the validation dataset. LAI measurements from the riparian areas were not used for this analysis.

Point data were retrieved from the NN-predicted LAI image using the geographic locations of the ground-truth LAI sample sites. However, due to unavoidable geo-registration errors and the close proximity of some of the sites to features such as roads, homesteads, and adjacent fields under different cropping systems, some of the retrieved LAI image pixels were either directly on or too close to unrepresentative surface features. These data points were considered to be outliers and were excluded from further analysis.

4. Results

Table 1 contains a summary of the LAI retrieval results. Comparisons of estimated versus measured LAI using the NDVI and GI empirical methods for July 1 and July 8 are plotted as Figs. 4a,b and 5a,b. Both NDVI and GI results for July 1 are considerably better than results obtained for July 8. Linear regressions of estimated versus measured LAI for

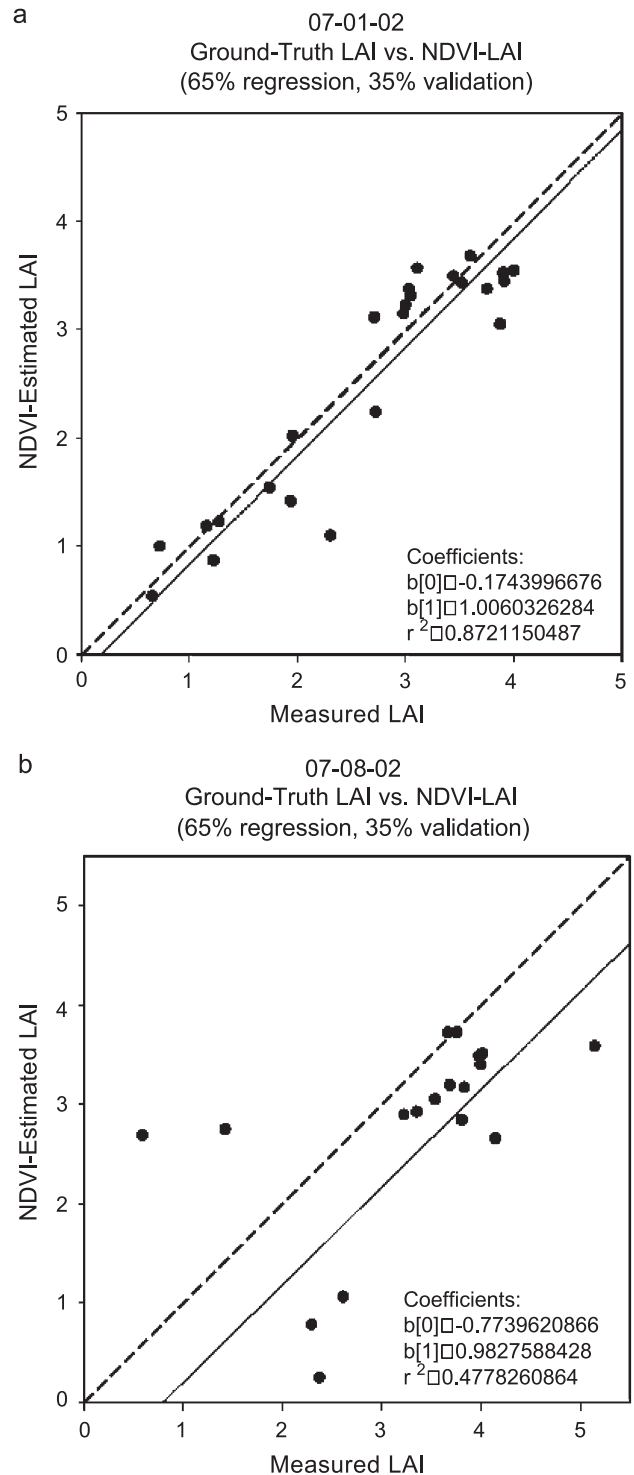


Fig. 4. (a) LAI-2000 ground measurements vs. LAI estimated from empirical NDVI approach for July 1 Landsat-7 ETM+ overpass. The solid line is the regression line ($r^2=0.87$) and the dashed line is the one-to-one line. (b) LAI-2000 ground measurements vs. LAI estimated from empirical NDVI approach for July 8 Landsat-7 ETM+ overpass. The solid line is the regression line ($r^2=0.48$) and the dashed line is the one-to-one line.

July 1 for both SVIs resulted in very small offsets from 0.0 and slopes close to the 1:1 line. For July 1, the r^2 for the NDVI is slightly higher than the r^2 for the GI while both

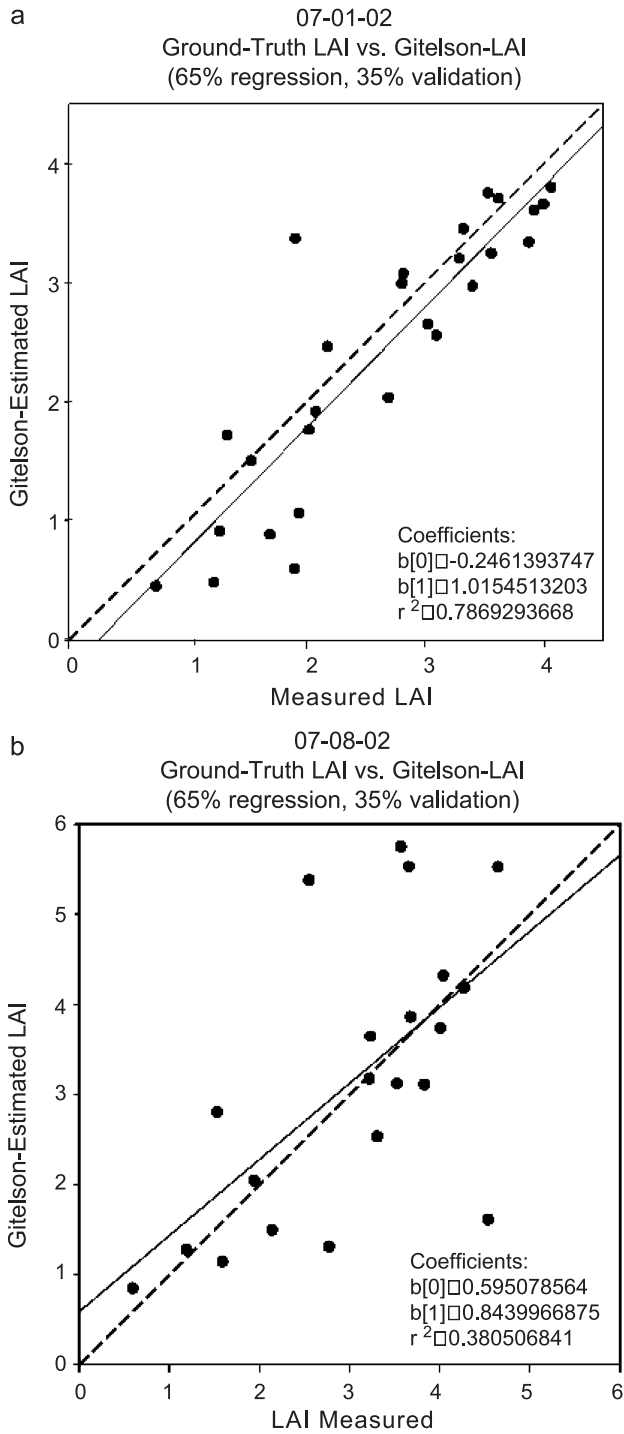


Fig. 5. (a) LAI-2000 ground measurements vs. LAI estimated from empirical Gitelson approach for July 1 Landsat-7 ETM+ overpass. The solid line is the regression line ($r^2=0.79$) and the dashed line is the one-to-one line. (b) LAI-2000 ground measurements vs. LAI estimated from empirical Gitelson approach for July 8 Landsat-7 ETM+ overpass. The solid line is the regression line ($r^2=0.38$) and the dashed line is the one-to-one line.

SVIs appear to overestimate higher LAI values and underestimate lower values. The comparisons for the July 8 date show a higher r^2 and slope closer to 1.0 for the NDVI than

for the GI. There is considerable scatter of the data for both dates.

The scaled NDVI measured versus estimated LAI results for both dates are shown as Fig. 6a and b. The July 1 comparison has a higher r^2 , a slope closer to 1.0, and a

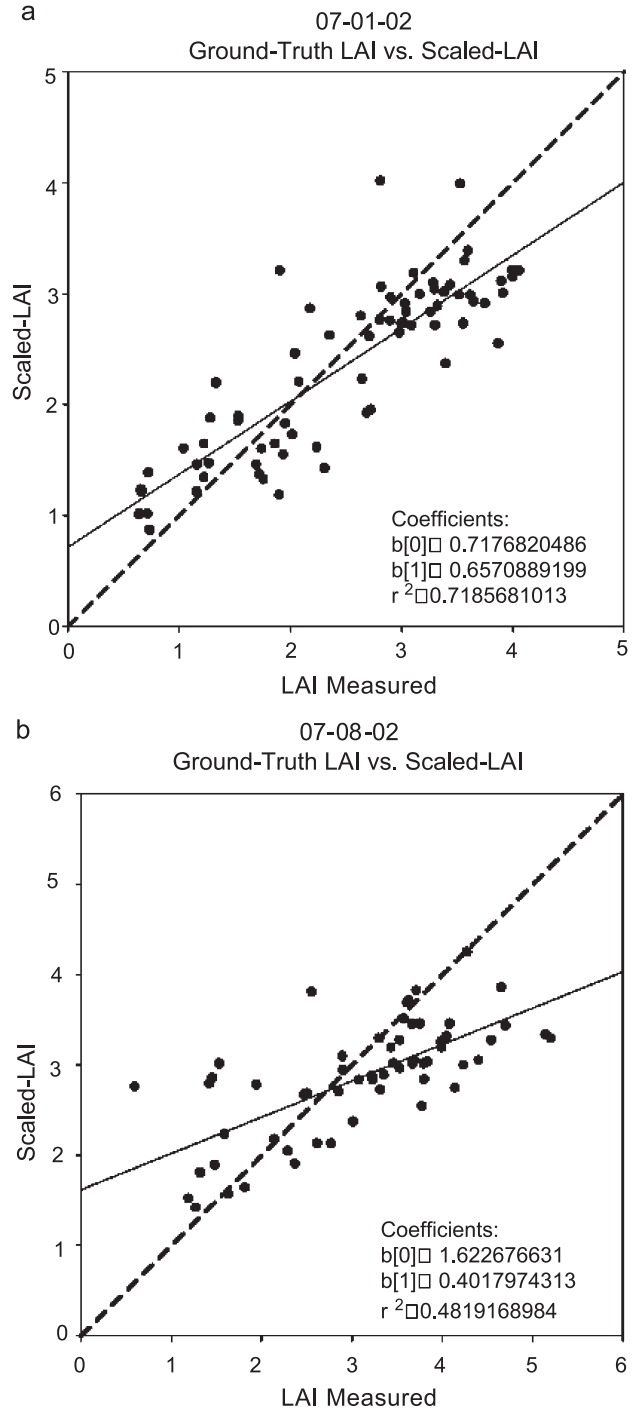


Fig. 6. (a) LAI-2000 ground measurements vs. LAI estimated from scaled approach for July 1 Landsat-7 ETM+ overpass. The solid line is the regression line ($r^2=0.72$) and the dashed line is the one-to-one line. (b) LAI-2000 ground measurements vs. LAI estimated from scaled approach for July 8 Landsat-7 ETM+ overpass. The solid line is the regression line ($r^2=0.48$) and the dashed line is the one-to-one line.

smaller offset from the origin than the July 8 comparison. Both dates show a tendency to overestimate lower LAI values and underestimate higher values. Note that the empirical NDVI and scaled NDVI approaches perform comparably within each date.

The measured versus estimated LAIs for both dates using the hybrid NN approach are shown as Fig. 7a and b. The r^2

is greater for the July 1 date and the slope is closer to the 1:1 line than the July 8 date. The offset from the origin for the July 8 comparison is slightly higher than the July 1 regression.

5. Discussion

Although all of the SVI methods out-performed the hybrid RT-NN method on July 1, it is significant that the RT-NN approach had the second highest r^2 on July 8 (0.40 versus 0.48) and that the scaled NDVI method performed reasonably well relative to the empirical SVI methods on the 1st (0.72 versus 0.79 and 0.87) and shared the highest r^2 for July 8 (0.48) with the NDVI approach. Note also that the changes of RMSE between July 1 and July 8 for the scaled NDVI and RT-NN methods were an order of magnitude less (0.4 and 0.7, respectively) than changes of the RMSE for the empirical SVI methods (0.74 and 0.82 for the GI and NDVI approaches, respectively).

Prior analysis of the RT-NN method showed that a reflectance error of $\pm 10\%$ causes an error of 0.41 LAI difference (Fang & Liang, 2003). The LAI error increases to 0.70 when the uncertainty of reflectance is $\pm 15\%$. The performance of the RT-NN process may be improved if model input parameters were estimated from direct field measurements. This, however, would run counter to one of the stated objectives of this analysis which is how to retrieve regional LAI estimates from satellite data without the need for site-specific, ground calibration measurements. For the purposes of this investigation, the RT-NN input parameters reported to be appropriate values for corn and soybeans were obtained from the literature. The lack of site-specific inputs directly measured in the field at the time of the satellite overpass did not produce unrealistic LAI retrieval values from the RT-NN or the scaled NDVI methods; in fact, the acceptable performance of these approaches suggests that literature values for model input parameters can suffice.

All of the LAI retrieval methods performed better for the July 1 imagery than for the July 8 imagery. The most notable differences between the dates that may have influenced LAI retrieval performance include availability of ground measurement datasets for the determination of LAI for the satellite overpass dates and the presence of smoke in the atmosphere on July 8. The inability to interpolate exact LAI values for the July 8 overpass due to the lack of any ground-truth LAI measurements acquired after the 8th would not seem to explain the significant differences noted between the two dates because all LAI retrieval results, including those lacking calibration measurements, showed decreased performance for July 8.

Another complicating factor is that by July 8 many of the corn plants would have tasseled, and tasseling is known to affect reflectance. The consistently lower r^2

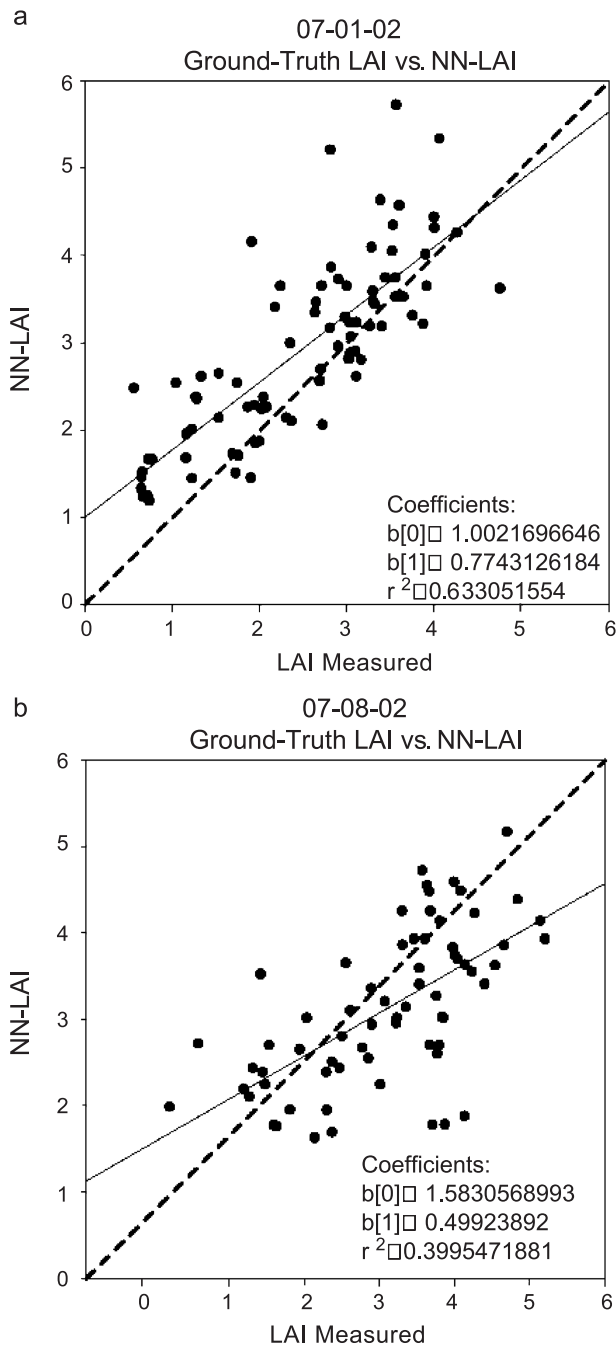


Fig. 7. (a) LAI-2000 ground measurements vs. LAI estimated from NN approach for July 1 Landsat-7 ETM+ overpass. The solid line is the regression line ($r^2=0.63$) and the dashed line is the one-to-one line. (b) LAI-2000 ground measurements vs. LAI estimated from NN approach for July 8 Landsat-7 ETM+ overpass. The solid line is the regression line ($r^2=0.40$) and the dashed line is the one-to-one line.

and higher RMSE for the July 8 data suggest that this imagery contains surface reflectance calculation errors and that the atmospheric corrections may not have accounted for the much higher atmospheric turbidity caused by the presence of smoke on this date. Investigations using MODIS and GOES imagery from SMEX02 acquired on July 8 have also encountered difficulty calculating surface reflectance. In situ near infrared surface reflectance measurements acquired with hand-held radiometers on July 8 showed reasonable agreement with satellite reflectances. However, in situ visible surface reflectance measurements were lower than satellite-based reflectance (P. Doraiswamy, personal communication). Increased visible reflectance would affect determination of the minimum and maximum soil reflectance values of the NN approach and calculation of NDVI for the scaled procedure. It is, however, notable that the RMSE for the scaled approach had a modest increase for the July 8 data. The NDVI and GI approaches would also be affected by brighter visible reflectance. Increased visible reflectance would be analogous to a decrease in vegetative cover and increasing soil exposure, thus introducing a bias.

The plots of estimated versus predicted LAI show interesting trends about the various retrieval methods. The NDVI and GI methods for July 1, conducted with site-specific in situ calibration measurements, show regression lines that are parallel to the 1:1 lines with a slight negative offset. This suggests that the calibrated methods do a reasonable job of estimating the full range of LAI of the study area.

The scaled and NN approaches of July 1, which lack site-specific in situ calibration measurements, show regression lines that cross the 1:1 lines with a positive offset. This trend also occurs for the July 8 scaled and NN approaches. This suggests that the uncalibrated methods perform reasonably well for mid-range LAI estimations while providing poorer estimates of lower and higher LAI values.

The July 8 NDVI method has a regression line that appears to follow the July 1 pattern. The July 8 GI method has a regression line that is very close to the 1:1 line, this time with a positive offset largely due to several high LAI outliers. Removal of the extreme outliers would shift the July 8 GI regression line closer to the 1:1 line.

Examination of the location of the outliers for all LAI retrieval approaches showed no obvious geographic trends or patterns. Stratification of the outliers according to whether LAI estimations were made for corn or soybean also showed no obvious trends. One sample site appeared as an outlier in three of the methods on July 1; another site was an outlier in three of the methods on July 8. This suggests that these validation measurements may not have corresponded with or were not adequately representative of the vegetative canopy conditions recorded by the satellite sensors.

6. Conclusions

The SVI methods—NDVI regression, GI regression, and scaled NDVI—appear to perform comparably. Plots of estimated versus measured LAI appear to suggest that the calibrated methods do a better job of estimating the full range of LAI values while the uncalibrated methods perform reasonably well for mid-range LAI estimations with less consistent estimation of higher and lower LAI values. While not performing as well as the SVI approaches, the hybrid RT-NN results are still impressive given that site-specific data for calibration or optimization of the MCRM are not needed.

The hybrid RT-NN approach is computationally complex as multiple analytical steps must be completed before an estimate can be produced. This method would be less cumbersome if LUTs could be produced and used to train the NN for many view angle/solar angle/soil brightness/growth stage scenarios before image acquisition and processing. The sensitivity of the procedure to the derivation of soil brightness inputs to the radiative transfer model via SRI suggests that further refinement of this procedure is warranted. The scaled NDVI and hybrid RT-NN methods raise issues concerning the choice of boundaries for determination of minimum and maximum image values. Implementation of a rigorous approach for avoiding the inclusion of water pixels and other outliers when selecting the minimum and maximum values would benefit these LAI retrieval approaches.

This study suggests that the most efficient method for LAI retrieval is the scaled NDVI approach as it does not require site-specific in situ measurements for calibration and uses simple formulae. However, the procedure does require a wide range of NDVI values to be present in the scene to properly pick minimum and maximum limits. Determination of the exponent in the f_c equation also warrants further investigation.

The results demonstrate that reasonable LAI estimates are possible using optical remote sensing methods without site-specific calibration measurements.

Acknowledgements

The authors gratefully acknowledge the efforts of numerous individuals responsible for collecting ground-based LAI measurements during SMEX02. Thanks are also extended to AERONET, especially Brent Holben and Wayne Newcomb, for the loan of the sunphotometer and the processing of the atmospheric optical properties data.

References

- Anderson, M. C., Neale, C. M. U., Li, F., Norman, J. M., Kustas, W. P., Jayanthi, H., & Chavez, J. (2004). Upscaling ground observations of vegetation cover and water content during SMEX02 using aircraft and Landsat imagery. *Remote Sensing of Environment*, 92, 447–464 (this issue).

- Baret, F., Jacquemoud, S., & Hanocq, J. F. (1993). The soil line concept in remote sensing. *Remote Sensing Review*, 7, 65–82.
- Best, R. G., & Harlan, J. C. (1985). Spectral estimation of green leaf area index of oats. *Remote Sensing of Environment*, 17, 27–36.
- Campbell, G. S., & Norman, J. M. (1998). *An introduction to environmental physics* (p. 268). New York: Springer-Verlag.
- Carlson, T. N., & Ripley, D. A. (1997). On the relation between NDVI, fractional vegetation cover, and leaf area index. *Remote Sensing of Environment*, 62, 241–252.
- Choudhury, B. J., Ahmed, N. U., Idso, S. B., Reginato, R. J., & Daughtry, C. S. T. (1994). Relations between evaporation coefficients and vegetation indices studied by model simulations. *Remote Sensing of Environment*, 50, 1–17.
- Colombo, R., Bellingeri, D., Fasolini, D., & Marino, C. M. (2003). Retrieval of leaf area index in different vegetation types using high resolution satellite data. *Remote Sensing of Environment*, 86, 120–131.
- Eck, T. F., Holben, B. N., Reid, J. S., Dubovik, O., Smirnov, A., O'Neill, N. T., Slutsker, I., & Kinne, S. (1999). Wavelength dependence of the optical depth of biomass burning, urban, and desert dust aerosols. *Journal of Geophysical Research*, 104, 31333–33349.
- Eklundh, L., Harrie, L., & Kuusk, A. (2001). Investigating relationships between Landsat ETM+ sensor data and leaf area index in a boreal conifer forest. *Remote Sensing of Environment*, 78, 239–251.
- Engman, E. T., & Chauhan, N. (1995). Status of microwave soil moisture measurements with remote sensing. *Remote Sensing of Environment*, 51, 189–198.
- Fang, H., & Liang, S. (2003). Retrieving leaf area index with a neural network method: Simulation and validation. *IEEE Transactions on Geoscience and Remote Sensing*, 41, 2052–2062.
- Fang, H., Liang, S., & Kuusk, A. (2003). Retrieving leaf area index using a genetic algorithm with a canopy radiative transfer model. *Remote Sensing of Environment*, 85, 257–270.
- Gillies, R. R., & Carlson, T. (1995). Thermal remote sensing of surface soil water content with partial vegetation cover for incorporation into climatic models. *Journal of Applied Meteorology*, 34, 745–756.
- Gitelson, A. A., Vina, A., Arkebauer, T. J., Rundquist, D. C., Keydan, G., & Leavitt, B. (2004). Remote estimation of leaf area index and green leaf biomass in maize canopies. *Journal of Plant Physiology*, 161, 165–173.
- Holben, B. N., Eck, T. F., Slutsker, I., Tanre, D., Buis, J. P., Setzer, A., Vermote, E., Reagan, J. A., Kaufman, Y. J., Nakajima, T., Lavenu, F., Jankowiak, I., & Smirnov, A. (1998). AERONET—a federated instrument network and data archive for aerosol characterization. *Remote Sensing of Environment*, 66, 1–16.
- Jackson, T. J., (Ed.). (2002). *Soil moisture experiments in 2002 (SMEX02): Experiment plan*. Available at: <http://hydrolab.arsusda.gov/smex02/>.
- Jacquemoud, S., Bacour, C., Poilve, H., & Frangi, J. -P. (2000). Comparison of four radiative transfer models to simulate plant canopies reflectance: Direct and inverse mode. *Remote Sensing of Environment*, 74, 471–481.
- Jacquemoud, S., & Baret, F. (1990). PROSPECT: A model of leaf optical properties spectra. *Remote Sensing of Environment*, 34, 75–91.
- Jacquemoud, S., Baret, F., Andrieu, B., Danson, F. M., & Jaggard, K. (1995). Extraction of vegetation biophysical parameters by inversion of the PROSPECT+SAIL models on sugar beet canopy reflectance data. Application to TM and AVIRIS sensors. *Remote Sensing of Environment*, 52, 163–172.
- Kimes, D. S., Nelson, R. F., Manry, M. T., & Fung, A. K. (1998). Attributes of neural networks for extracting continuous vegetation variables from optical and radar measurements. *International Journal of Remote Sensing*, 19, 2639–2663.
- Kuusk, A. (1994). A multispectral canopy reflectance model. *Remote Sensing of Environment*, 50, 75–82.
- Kuusk, A. (1995). A Markov chain model of canopy reflectance. *Agricultural and Forest Meteorology*, 76, 221–236.
- Li-Cor. (1992). *LAI-2000 plant canopy analyzer operating manual*. Lincoln, NE: Li-Cor.
- Myneni, R. B., Maggion, S., Jaquinta, J., Privette, J. L., Gobron, N., Pinty, B., Kimes, D. S., Verstraete, M. M., & Williams, D. L. (1995). Optical remote sensing of vegetation: Modeling, caveats, and algorithms. *Remote Sensing of Environment*, 51, 169–188.
- Price, J. C. (1990). On the information content of soil reflectance spectra. *Remote Sensing of Environment*, 33, 113–121.
- Rouse, J. W., Haas, R. H., Schell, J. A., & Deering, D. W. (1973). Monitoring vegetation systems in the Great Plains with ERTS. *Third ERTS Symposium, NASA SP353* (pp. 309–317). Washington, DC: USGPO.
- Smith, J. A. (1993). LAI inversion using a back-propagation neural network trained with a multiple scattering model. *IEEE Transactions on Geoscience and Remote Sensing*, 31, 1102–1106.
- Spanner, M. A., Pierce, L. L., Running, S. W., & Peterson, D. L. (1990). The seasonality of AVHRR data of temperate coniferous forests: Relationship with leaf area index. *Remote Sensing of Environment*, 33, 97–112.
- Venables, W. N., & Ripley, B. D. (1994). *Modern applied statistics with S-Plus* (pp. 261–266). New York: Springer-Verlag.
- Vermote, E. F., Tanre, D., Deuze, J. L., Herman, M., & Morcrette, J. J. (1997). Second simulation of the satellite signal in the solar spectrum, 6S: An overview. *IEEE Transactions on Geoscience and Remote Sensing*, 35(3), 675–686.
- Verstraete, M. M., Pinty, B., & Myneni, R. B. (1996). Potential and limitations of information extraction on the terrestrial biosphere from satellite remote sensing. *Remote Sensing of Environment*, 58, 201–214.
- Welles, J. M. (1990). Some indirect methods of estimating canopy structure. *Remote Sensing Reviews*, 5(1), 31–44.
- Welles, J. M., & Norman, J. M. (1991). Instrument for indirect measurement of canopy architecture. *Agronomy Journal*, 83(5), 818–825.